Internal geophysics (Applied geophysics)

Monitoring water flow in a clay-shale hillslope from geophysical data fusion based on a fuzzy logic approach

Gilles Grandjean [a,*], Clément Hibert [a], François Mathieu [a],
Emilie Garel [b], Jean-Philippe Malet [c]

[a] BRGM, service risques naturels et sécurité stockage CO2, 3, avenue Claude-Guillemin, BP 36009, 45060 Orléans, France
[b] Environnement méditerranéen et modélisation des agro-hydrosystèmes, faculté des sciences,
université d'Avignon et des pays de Vaucluse, 33, rue Louis-Pasteur, 84000 Avignon, France
[c] School and observatory of Earth Sciences, Institute of Earth physics, University of Strasbourg,
5, rue Descartes, 67084 Strasbourg, France

Abstract

Seismic and electrical resistivity tomography allow subsurface characterization from acoustic P-waves (Vp), shear S-waves (Vs) velocities, and electrical resistivity (ρ). Both geophysical methods were used to monitor water flow during a controlled rainfall experiment on a clay-shale hillslope located in the Laval catchment at Draix (Alpes-de-Haute-Provence, France). The objectives of the rainfall experiment were to analyse the water infiltration processes and identify possible water pathways by combining multi-method observations. The seismic data provide information on fissure density and the electrical resistivity data provide information on soil water content within the hillslope. Changes of the Vp and electrical resistivity fields with time show some similar pattern. To go further in the analysis of the water flow a geophysical data fusion strategy based on fuzzy set theory is applied. The computed fuzzy cross-sections based on expert hypotheses show the possibility for the material to be saturated during the rainfall experiment. The data fusion process is repeated in time for each acquisition set. The relative difference between the obtained fuzzy cross-sections is calculated and reveals possible locations where water may be transferred within the hillslope. *To cite this article: G. Grandjean et al., C. R. Geoscience 341 (2009).*

© 2009 Académie des sciences. Published by Elsevier Masson SAS. All rights reserved.

Résumé

Surveillance des écoulements d'eau sur une pente de colline schisto-argileuse à partir de fusion de données géophysiques par logique floue. Les méthodes de tomographie sismique et électrique permettent de caractériser les matériaux de la subsurface à partir des vitesses sismiques des ondes P (Vp) ou S (Vs) et de la résistivité électrique (ρ). Ces deux méthodes ont été mises en œuvre pour suivre les écoulements d'eau pendant une expérience de pluie contrôlée sur un versant marneux localisé dans le bassin versant du Laval à Draix (Alpes-de-Haute-Provence, France). L'objectif de l'expérimentation en pluie simulée était d'analyser le processus d'infiltration et d'identifier des chemins d'écoulement préférentiel, au sein du versant, par une approche multiméthode. Les champs de vitesse Vp et de résistivité électrique ρ fournissent une information complémentaire, respectivement sur l'état de fissuration du versant, et sur les variations de teneur en eau en subsurface. Une méthode de fusion de données par

* Corresponding author.
  E-mail address: g.grandjean@brgm.fr (G. Grandjean).

logique floue est ensuite utilisée pour représenter l'information de manière plus objective et compréhensible par des non spécialistes. Les calculs sont fondés sur des hypothèses de saturation partielle ou totale du versant, et permettent de suivre la progression de la saturation en eau pendant la pluie simulée. La différence entre les sections de possibilité calculées pour chaque pas de temps permet de localiser des chemins d'écoulements préférentiels dans le versant. ***Pour citer cet article : G. Grandjean et al., C. R. Geoscience 341 (2009).***

1. Introduction

Erosion of clay-shale sediments (e.g. Callovo-Oxfordian black marls), which cover a large area in Southeast France, results in dam fillings all along the Durance River down to the ''*Etang de Berre*'' on the Mediterranean Coast. In the high-energy landscapes of this area, slope failures may occur and contribute to the sediment transport from the hillslopes to the rivers [2,3].

The objective of this work is to analyze the hydrological processes on a badland slope characterized by reworked and weathered soil material. The infiltration process has been studied on a slope instrumented with several hydrological devices (soil water content sensors, tensiometers, suction lysimeters and piezometers) and geophysical methods during a large-scale infiltration experiment. A method for characterizing soil moisture distribution and the water flow pattern within the hillslope is proposed by combining several geophysical parameters with the Fuzzy Set theory.

Non-intrusive and indirect geophysical methods (such as seismic refraction and electrical resistivity imaging) are well adapted for analysing the characteristics of clay-shale hillslopes [17,24]. The joint interpretation of acoustic P-wave velocity (V_p), S-wave velocity (V_s) and electrical resistivity (ρ) can reveal hydrological and geomechanical properties. According to previous studies [7,19] a multi-method approach is proposed to deepen the level of information, assuming that:

- V_p and V_s are more particularly sensitive to the geomechanical characteristics and the fissure density of the soil [8];
- ρ is strongly dependent on water content of the porous media [23].

Grandjean et al. [12] have studied the correlation between V_p and ρ on the Super-Sauze mudslide, developed in the same lithology. This work showed that a cross-plot V_p-ρ reveals several possible hydro-geomechanical behaviours. These authors noticed the increase of V_p and ρ values in relation to a decrease in fissure density, and an increase of soil water saturation respectively. These results were used to propose a new objective method using the Fuzzy Set theory to combine the different geophysical parameters [13]. This method is applied in this work in order to determine possible water flow pathways, the timing of water infiltration and the pattern of soil water content in the soil.

The experimental hillslope (Fig. 1) is located in the Laval catchment, one of the tributary of the Bouinenc and Bléone rivers, near Draix (Alpes-de-Haute-Provence, France). This catchment has a characteristic badland type morphology with multiple V-shape gullies (Fig. 1a). The Laval catchment is instrumented by Cemagref for monitoring and studying erosion and sediment transport in black marl landscapes since 1984 [25]. The instrumented hillslope corresponds to a shallow slide triggered in December 1999 [7]. The elevation ranges from 850 m to 975 m, for an average slope of around 58%, and a surface of 0.04 km^2. The slide has a characteristic morphology associating a main scarp with plane rupture plans and an accumulation zone composed of reworked marls and blocks of heterogeneous sizes. The lithology is made of a heterogeneous clay-rich clastic matrix possibly highly saturated in water during the wet season [1]. This accumulation zone is both a water reservoir which can supply a baseflow to the main channel for some days after intense or prolonged rain events [3], and can strongly contribute to the high sediment yield observed in these catchments [25]. A more quantitative understanding of the hydrological processes observed in these hillslopes is of paramount importance to forecast water discharge and sediment transport in these landscapes [16].

2. Geophysical investigations

The geophysical investigations have been carried out using high resolution seismic and electrical instruments
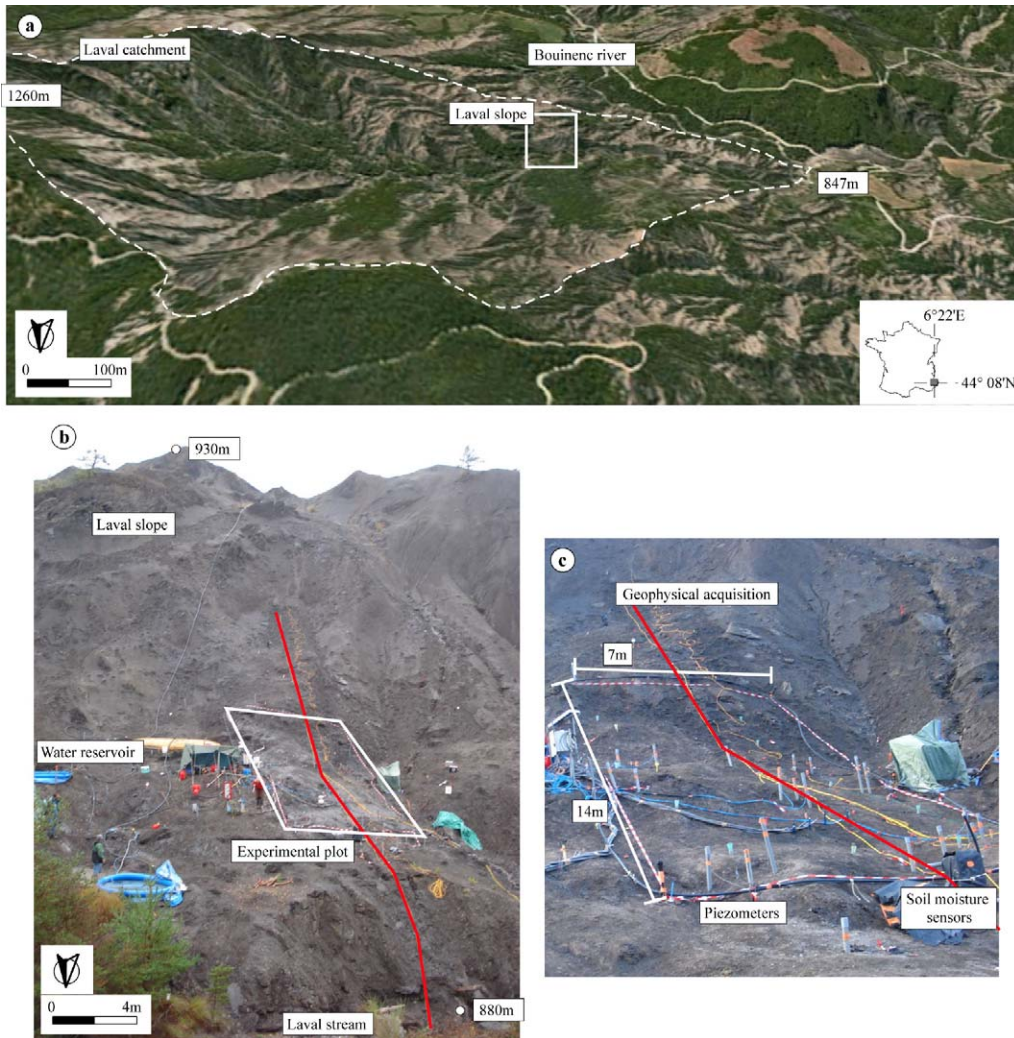
Fig. 1. Main geomorphological features of the instrumented hillslope. a: location of the instrumented slope in the Laval catchment at Draix (Alpes-de-Haute-Provence); b: photograph of the Laval slope and location of the experimental plot (the geophysical profile is indicated in red); c: photograph of the experimental plot with the location of the piezometer array and the soil moisture sensors.

Fig. 1. Caractéristiques géomorphologiques du versant étudié. a : localisation du versant instrumenté dans le bassin-versant du Laval à Draix (Alpes-de-Haute-Provence) ; b : photographie du versant du Laval et localisation de la parcelle d'infiltration (le profil géophysique est indiqué en rouge) ; c : photographie de la zone d'infiltration et localisation du réseau de piézomètres et de capteurs de teneurs en eau.

spread along a 48 m long profile located in the central part of a rainfall experiment plot of about 100 m^2 (7 × 14 m; Fig. 1b; Fig. 1c). Water enriched in bromide and chloride has been used during the experiment. A rainfall amount of 680 mm has been applied during 67 h, corresponding to a rainfall intensity of around 10 mm.h^{-1}. The soil profile was unsaturated at the start of the experiment (t_0).

During the rain experiment, geophysical measurements were performed with a time resolution of 3 h, according to Fressard et al. [7]. Then, time series of geophysical tomograms representing 2D-sections of V_p,

V_s and ρ values were calculated. The reliability of the inverted parameters was estimated by means of likelihood functions computed from *a posteriori* errors. The acquisition device, the inversion method and the method to estimate the likelihood functions are described in the following sections.

2.1. Seismic P-wave tomography

The acquisition system involved 48 channels seismic equipment featured by 40 Hz geophones and a handy-hammer source. Seismic shots were fired at each
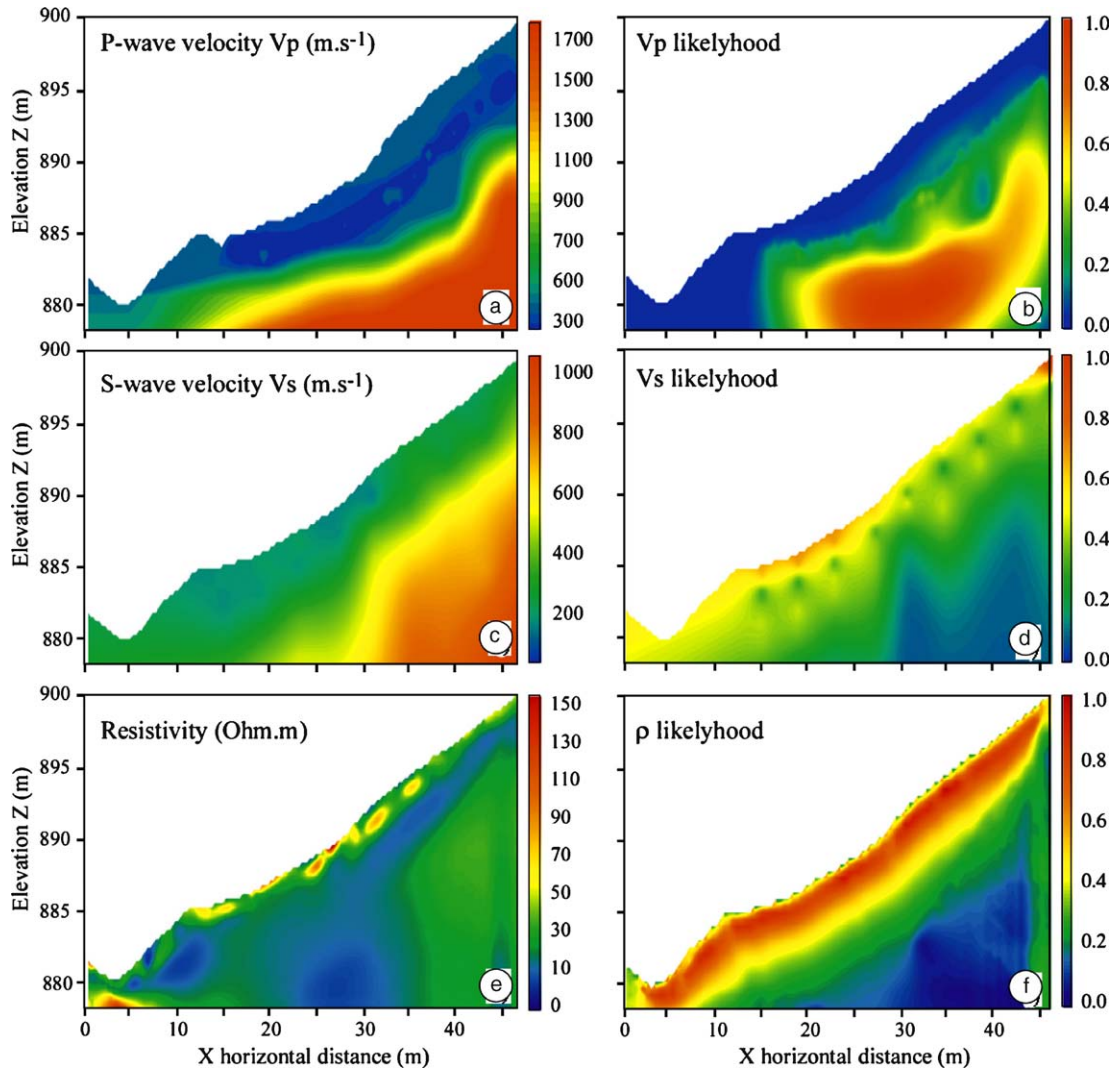
Fig. 2. Inverted geophysical tomograms. a: P-waves velocity tomography (V_p) inverted from the seismic first arrivals; b: V_p likelihood function (L_{V_p}) indicating the places where the inverted velocities are reliable; c: S-wave velocity tomography (V_s) inverted from SASW; d: V_s likelihood function (L_{V_s}) indicating the places where the inverted velocity values are reliable; e: Electrical tomography (ρ) inverted from apparent resistivity values; f: ρ likelihood function (L_{V_ρ}) indicating the places where the inverted resistivity values are reliable.

Fig. 2. Tomogrammes géophysiques inversés. a : tomographie de V_p inversée à partir des premiers temps d'arrivée sismiques ; b : fonction de vraisemblance pour V_p (L_{V_p}) indiquant les lieux où l'inversion est contrainte; c: Tomographie de V_s inversée par SASW ; d : fonction de vraisemblance pour V_s (L_{V_s}) indiquant les lieux où l'inversion est contrainte ; e : tomographie de ρ inversée à partir des valeurs de résistivité apparente ; f : fonction de vraisemblance ρ (L_{V_ρ}) indiquant les lieux où l'inversion est contrainte.

geophone, every meter. Data processing and inversion of the first arrival travel time were undertaken using the JaTS seismic tomography software [9,11]. Inverted V_p along the profile shows a three layer structure varying from 300 to 1800 m.s^{-1} (Fig. 2a): on top, a low-velocity layer with velocities ranging from 300 to 600 m.s^{-1}, in intermediate position, a thinner layer with velocities ranging from 600 to 1200 m.s^{-1}, and at depth a layer with high velocities, ranging from 1200 to 1800 m.s^{-1}. According to the geotechnical investigation carried out

by Fressard et al. [7], the two first layers correspond to the reworked and accumulated material, and the third layer correspond to the marly bedrock [19,20]. In order to focus the interpretation on well-resolved zones of the mudslide, the likelihood L_{V_p}, equivalent to a correlation function, has been estimated (Fig. 2b). It corresponds here to the sum of elementary Fresnel weights featuring each source-receiver pair weighted by the normalized RMS value obtained at the final iteration of the inversion process [13]. After processing seismic data for

all time steps, no travel-time difference induced by the increasing saturation of the soil was observed on the time-varying tomograms, indicating that seismic wave propagation should not be used alone to monitor water flow in the mudslide.

2.2. Spectral analysis of surface waves (SASW)

SASW is of increasing interest in the geophysical community [29] because it is a non-invasive method to evaluate soil stiffness with depth in terms of V_s soundings [22]. This method can be easily implemented along linear profiles to obtain two-dimensional V_s sections of shallow layers [21]. Before the inversion step, each seismic record needs to be transformed into a dispersion image from which the frequency-phase velocity curve (e.g. dispersion curve) is estimated. In laterally contrasted media, dispersion images need to be computed in a more local manner with respect to the 1D assumption required by the inversion method proposed by Herrmann [15]. To overcome this problem, the 2M-SASW (Multifold Multichannel SASW) technique [10] has been performed on the same seismic data used previously for the P-waves tomography. S-waves soundings, computed for each local dispersion curve, were finally interpolated along the seismic profile by using kriging algorithms (Fig. 2c). Likelihood values L_{Vs} related to inverted V_s soundings were directly estimated from the diagonal values of the correlation matrix defined in the inverse problem [15] and interpolated (as for the V_s soundings) to be represented on 2D sections (Fig. 2d).

2.3. Electrical resistivity tomography

The electrical apparent resistivity profile was performed along the same profile, using a Wenner-Schlumberger array. The profile was also 48 m long, and electrodes were 1 m apart. Data processing and inversion steps were carried out according to Loke [18] by implementing a damped least-squared Gauss-Newton algorithm. The inverted tomograms show a very low resistivity and few contrasted values of resistivity, ranging from 10 ς.m in the central part of the profile to 150 ς.m at the surface. Lateral variations are also observed, with a resistivity going from 20 ς.m to 150 ς.m in the topsoil (Fig. 2e). The reliability of the resistivity tomogram L_ρ has been computed from Loke's software outputs by considering the error ε on the inverted resistivity [13]. The image of Fig. 2f allows one to distinguish between high-reliability zones from those poorly constrained; the high reliability is mainly

restricted to the superficial part of the tomogram. The comparison of the tomograms observed at different time steps shows nevertheless some changes with time of the electrical resistivity.

2.4. Direct analysis of the geophysical parameters

In order to understand how the geophysical parameters are correlated, an analysis of V_p versus depth and ρ versus V_p has been carried out. For this purpose, data were extracted from the tomograms to compute virtual depth-soundings. Analysis of Fig. 3a and b indicates that:

- the V_p increases with depth (Fig. 3a), and this increase is probably linked to a decrease of fissure density with depth due to the development of tensile zones in the material [19,20];
- the more the virtual sounding is close to the upslope part of the experimental plot (e.g. increasing 'x' values), the higher the electrical resistivity (Fig. 3b). This observation could indicate that the upslope part of the cross-section is more unsaturated than the downslope part where water may accumulate.

In addition, many authors demonstrated that seismic velocities could be linked to soil porosity changes. Wyllie et al. [28] established the so-called time average relationship which is an empirical function defined by $1/V = A + B\Phi$ (with Φ, the porosity; A, B, some constant coefficients depending on lithology and pressure). This relationship is empirical but can be considered as valid when the effective pressure is high and the rock is saturated, as observed in this experiment. The A & B coefficients were not determined for black marls and no differential pressure measurements were taken during the experiment. Nevertheless, Dvorkin et al. [6] showed that a V_s–V_p cross-plot for marly rocks made from well-log data fits correctly experimental cross-plots originally designed for calcite. In addition, Domenico [4] demonstrated that in calcite-rich rocks, the difference ($\Delta = 1/V_s - 1/V_p$) is sensitive to porosity changes: the higher this difference, the more the medium is supposed to be porous. These considerations led us to work with a new quantity defined as the slowness difference of velocities that should represent the variation of porosity within the slope (Fig. 4). Areas with high ΔV values should highlight soil parts wherein the porosity is higher and consequently, portion of the terrain more able to conduct water.

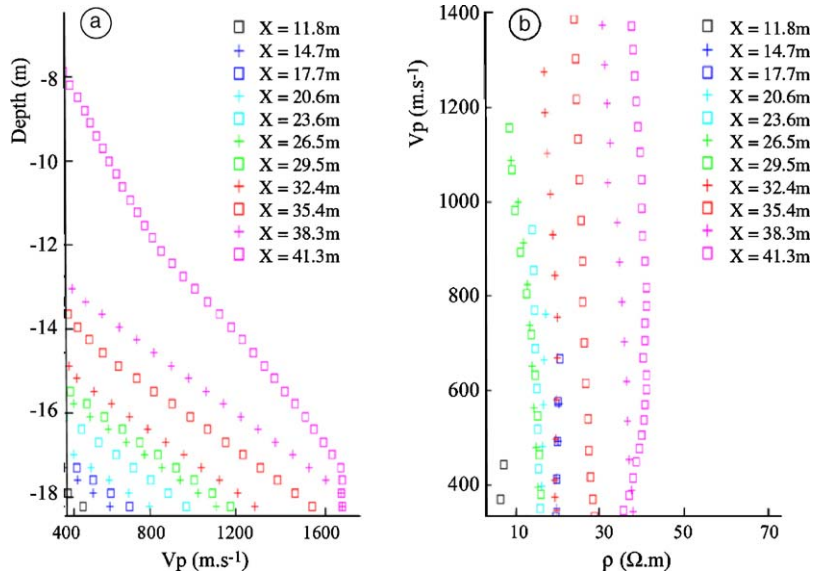These statements are used hereafter to define hypotheses for the fusion of the geophysical data.

Fig. 3. Changes in geophysical parameters. a: P-wave velocity variations with depth for several distances along the profile; b: P-wave velocity versus electrical resistivity for several vertical slices in the tomogram models.

Fig. 3. Variations des paramètres géophysiques. a : variation de la vitesse des ondes P en fonction de la profondeur pour différentes distances le long du profil ; b : variation de la vitesse des ondes P en fonction de la résistivité pour différentes distances le long du profil.
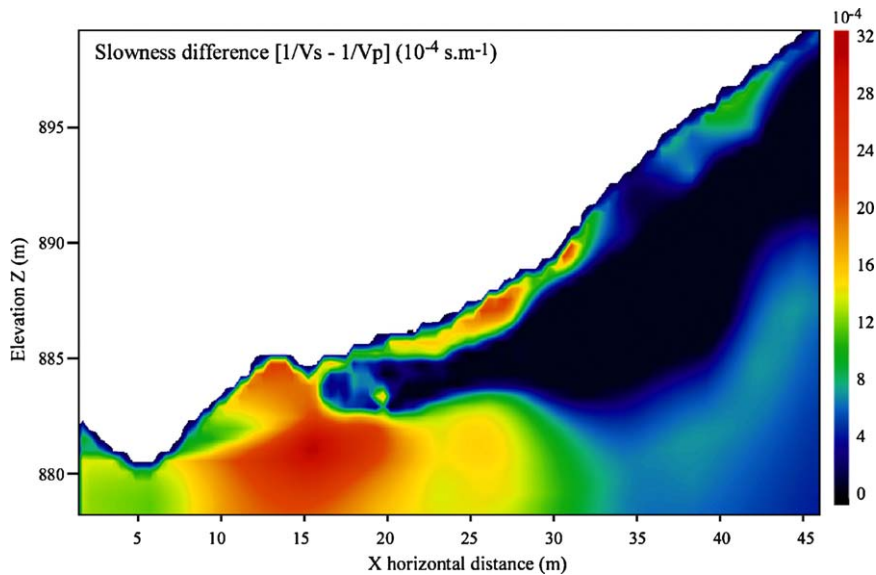

Fig. 4. Slowness difference plot ($1/V_s - 1/V_p$).

Fig. 4. Image de la différence des lenteurs sismiques ($1/V_s - 1/V_p$).

3. Fuzzy theory and proposed modelling strategy

One of the specificity of geophysical data comes from their uncertainty and inaccuracy when they are interpreted for geomorphological and geotechnical applications. Fortunately, different mathematical tools allow considering this specificity by modelling the data in terms of probability, evidence or possibility theories. In the following, probability theory is supposed to be known, and only the basics of the possibility theory are exposed as a new approach to handle the uncertainties

related to topic-oriented interpretation. A more complete demonstration on this issue is detailed in Grandjean et al. [13].

The possibility theory has been introduced by Zadeh [30] and fully presented by Dubois and Prade [5] and Zimmermann [31]. The possibility theory considers a reference space S defined in R^n, and a subset X of S defined by a belonging function π (Eq. (1)):

$$\pi(x) = \begin{cases} 1 & \text{if} \quad x \in X \\ 0 & \text{if} \quad x \notin X \end{cases} \tag{1}$$

If we attribute to the subset X the realization of a given hypothesis, the belonging function reveals the possibility that this hypothesis is realized depending on the values of x. Furthermore, the fuzzy theory states that intersection and union of two fuzzy sets can be defined by the minimum (min) and maximum (max) of the belonging function π_1 and π_2:

$$\forall x \in S, \quad \begin{cases} (\pi_1 \cap \pi_2)(x) = \min[\pi_1(x), \pi_2(x)] \\ (\pi_1 \cup \pi_2)(x) = \max[\pi_1(x), \pi_2(x)] \end{cases} \tag{2}$$

A possibility distribution is a function π defining the belonging of each element of S to the realisation of the hypothesis: according to Eq. (1) and Eq. (2), $\pi(x)$ is equal to 1 or 0 depending if the hypothesis is realized or not, respectively. This assumption leads mathematically to Eq. (3):

$$\begin{aligned} &\pi : S \rightarrow [0, 1] \\ &\sup(\pi(x)) = 1 \end{aligned} \tag{3}$$

Another interesting contribution of this approach is the formalism allowing the functions to be combined by the mean of appropriate operators. According to Eq. (2), the combination of two possibility distributions is given by Eq. (4):

$$\pi(x) = \pi(x)1 \oplus \pi(x)2 = \frac{\pi 1(x) \wedge \pi 2(x)}{\sup(\pi 1(x) \wedge \pi 2(x))} \tag{4}$$

where $\wedge$ is the intersection operator.

Coming back to our geophysical dataset, the problem consists in applying fusion theory to increase the amount of information from each geophysical tomogram without overestimating the quality and reliability of the results. Therefore, the datasets, hypotheses and meta-hypotheses are defined as follows:

- the datasets refer to the seismic velocities and the resistivity tomograms (Fig. 2a, c, e) featured by their likelihood spatial distributions;
- the hypotheses refer to several interpretations derived from the geophysical data. They are qualitative and

define the possibility functions π. For example, if some fissures exist in the slope when the V_p values are lower than the limit V_{pL}, the hypothesis "the soil is fissured" represented by π will be equal to 1 if the V_p value is lower than V_{pL} ;
- the meta-hypotheses result from a fusion of the elementary hypotheses and define the belonging of each spatial element to different hydrological interpretations.
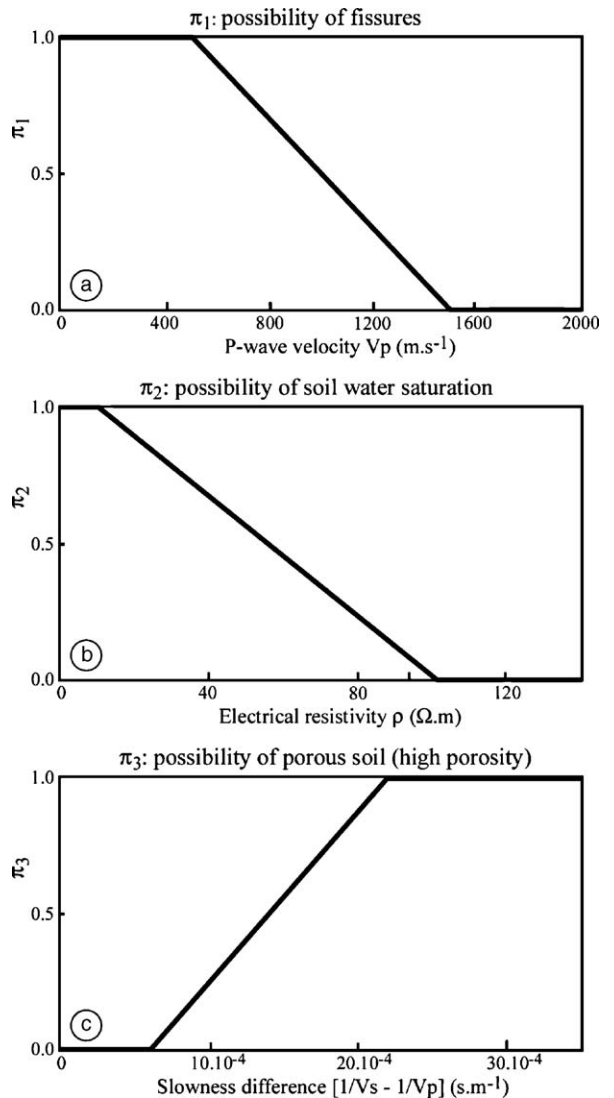

Fig. 5. Belonging functions describing the possibility distributions π_1, π_2 and π_3 corresponding to the three tested hypotheses. a: h_1 – "possibility of fissures"; b: h_2 – "possibility of water saturation"; c: h_3 – "possibility of high soil porosity".

Fig. 5. Fonctions d'appartenance décrivant les lois de possibilité pour les trois hypothèses testées : a : h_1 – « possibilité pour le sol d'être fissuré » ; b : h_2 – « possibilité pour le sol d'être saturé en eau »; c : h_3 – « possibilité de sol à forte porosité ».

By comparing field observations and the inverted geophysical tomograms, it is possible to construct hypotheses on the terrain properties by affecting V_p, V_s or ρ values to observed material behaviours. For example, the bedrock identified from geotechnical soundings characterized on the V_p tomogram by the condition $V_p > 1500$ m.s^{-1}. This was used to identify thresholds values defining the possibility functions expressed by Eq. (1) and represented in Fig. 5:

- hypothesis h_1 defines the possibility π_1 that the soil is affected by fissures due to the deformation. The density of fissures is correlated to the variation of V_p observed at the subsurface. Geomorphological observations indicate that the soil may be considered respectively as fissured and not fissured if the V_p is lower than 300 m.s^{-1} and greater than 1500 m.s^{-1}. The possibility function is assumed to vary linearly between these two values (Fig. 5a);
- hypothesis h_2 defines the possibility π_2 of the soil to be saturated with water according to the observed value of electrical resistivity. From *in situ* soil moisture measurements available in the topsoil, the soil is considered respectively as saturated and unsaturated if the electrical resistivity is lower than 10 ς.m and greater than 100 ς.m. The possibility is assumed to vary linearly between these two values (Fig. 5b);

fusion of a possibility and a likelihood function is expressed by Eq. (5):

$$\pi * (x) = \pi(x) \vee (0.5 - L(x)) = \max(\pi(x), 0.5 - L(x)) \tag{5}$$

where $\vee$ is the union operator, $\pi(x)$ refers to the possibility functions defined in (Eq. (3)), $L(x)$ refers to the distribution of the likelihood values computed for each inversion processes, and x is the spatial reference of tomograms. We can note that for likelihood values set to zero, $\pi*$ drops to a value of 0.5 indicating that this hypothesis has an equi-possibility to be realized in case of no reliable data.

4. Application to the experimental plot on the Laval hillslope

4.1. Interpretation before the start of the rain experiment

The methodology has first been applied to identify the areas within the slope where the soil characteristics may favour infiltration. Two fusion models were computed: the first model combines ρ and V_p; the second model combines V_p, ρ and the slowness differences Δ in order to highlight the possible location of saturated zones. In a first step, hypotheses h_1, h_2 and h_3 were implemented using (Eq. 5). The implementation is defined by (Eq. (6)):

$$\begin{cases} \pi_1^*(Vp(x,z)) = \pi_1(Vp(x,z)) \vee (0.5 - L_p(x,z)) = \max(\pi1(x), 0.5 - L_{Vp}(x,z)) \\ \pi_2^*(\rho(x,z)) = \pi_2(\rho(x,z) \vee (0.5 - L_\rho(x,z)) = \max(\pi2(x,z), 0.5 - L_\rho(x,z)) \\ \pi_3^*(\Delta(x,z)) = \pi_3(\Delta(x,z) \vee (0.5 - L_\Delta(x,z)) = \max(\pi3(x,z), 0.5 - L_\Delta(x,z)) \end{cases} \tag{6}$$

- hypothesis h_3 defines the possibility π_3 of the soil to have a relatively higher porosity than the supposed average porosity of the reworked soil. According to the slowness model, the soil should have respectively a relative low porosity and high porosity for slowness differences of 0.00055 s.m^{-1} and 0.0022 s.m^{-1}. The possibility is assumed to vary linearly between these two values (Fig. 5c).

The relevance of the strategy, based on the three above-cited hypotheses, is controlled by the definition of the belonging functions [13]. The thresholds in the values defining the belonging functions were checked with field observations when available, petrophysics values and charts otherwise [14,26].

The last information that needs to be integrated concerns the likelihood functions. In our approach, the

where (x,z) refers to the spatial coordinates of the tomograms. These quantities were then combined by applying (Eq. (4)) in order to define meta-hypotheses H*, e.g. a combination of the elementary hypotheses h_1, h_2 or h_3. These new quantities can be considered as arbitrary but may represent a connection between the quantitative approach of geophysics and the necessity for engineering geologists to obtain an integrated diagnosis. The meta-hypotheses $H*_1$ and $H*_2$ are explained hereafter:

- Meta-hypothesis $H*_1$ defines the possibility for the soil to be saturated in water (e.g. low resistivity values) and to be highly affected by fissures (e.g. low V_p values). In terms of possibility theory, the meta-hypothesis $H*_1$ may be expressed by a function Π_1:
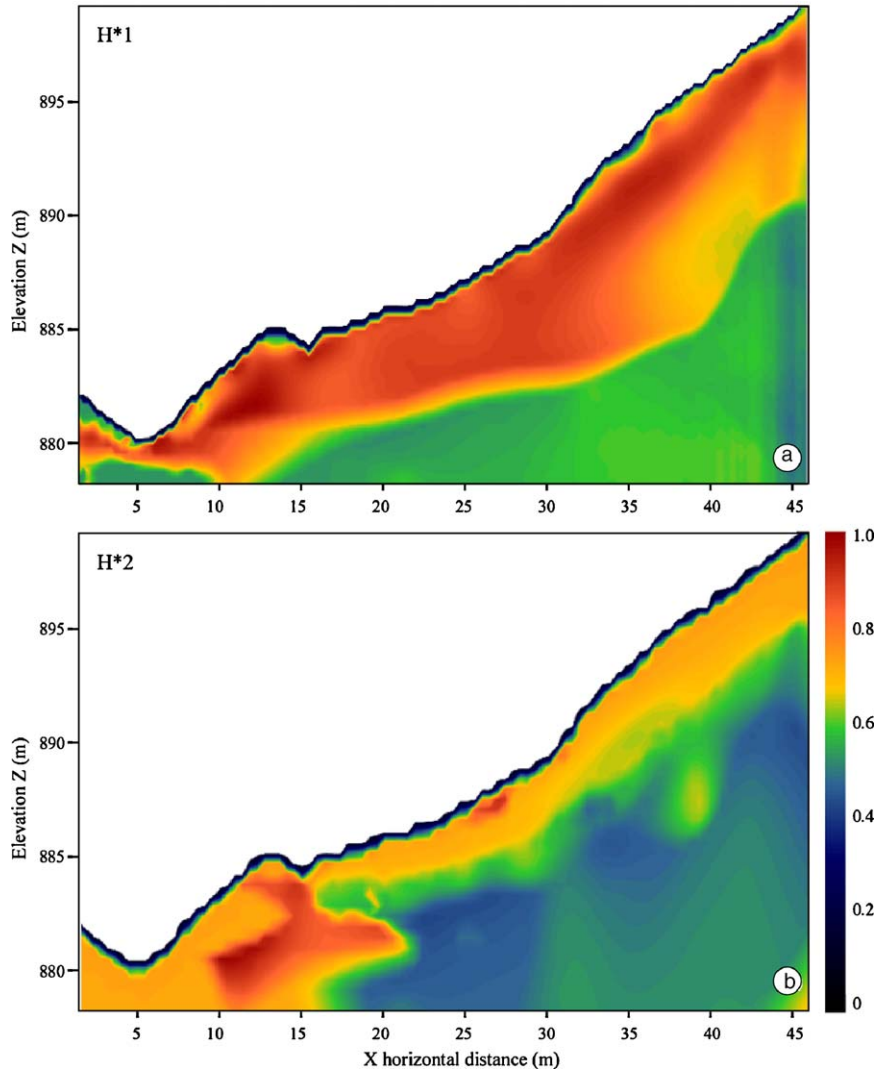
$$\Pi_1 = \pi_1^* \oplus \pi_2^* \tag{7}$$

Fig. 6. Distribution of possibility values indicating where the meta-hypotheses are realized. a: Meta-hypothesis H*$_1$; b: Meta-hypothesis H*$_2$. H*$_1$ was computed with V$_p$ and ρ parameters using π1 and π2 elementary hypotheses; H*$_2$ was computed with V$_p$, ρ and Δ parameters, using π1, π2 and π3 elementary hypotheses.

Fig. 6. Distribution des valeurs de possibilités pour la réalisation des méta-hypothèses. a : méta-hypothèse H*$_1$; b : méta-hypothèse H*$_2$. H*$_1$ a été calculée avec V$_p$ et ρ, en utilisant les hypothèses π1 et π2; H*$_2$ a été calculée avec V$_p$, ρ et Δ, en utilisant les hypothèses π1, π2 et π3.

Fig. 6a shows the result when (Eq. (7)) is solved. It indicates a superficial layer with a possibility value comprised between 0.8 and 1.0 overlying soil strata with lower possibility values ranging from 0.4 to 0.6. The shallow layer has a heterogeneous thickness going from 0.1 m at the toe of the slope to ca. 10 m at a distance of 35 m from the toe. As a consequence, a large amount of water should be able to flow within this top layer. The lower layer can be interpreted as the bedrock of the landslide from a geotechnical point of view.

• Meta-Hypothesis H*$_2$ defines the possibility for the soil to be saturated by water, to be highly affected by fissures and to have a relatively high porosity. In terms of possibility theory, the meta-hypothesis H*$_2$ may be expressed by the function Π_2:

$$\Pi_2 = \Pi_1 \oplus \pi_3^* \tag{8}$$

The section computed from (Eq. (8)) and displayed on Fig. 6b is more constrained than the section on Fig. 6a. Indeed, the V$_p$ is correlated to the presence of

fissures but is relatively unaffected by the degree of water saturation. Consequently, the model presented on Fig. 6b discriminates well-saturated and highly fissured zones from unsaturated and highly fissured zones. The introduction of the slowness difference in the fusion model has refined the location of the possible saturated zones in the topsoil. Relevant information can be extracted from this image: between distance 17 and 46 m, the possibly saturated layer is 1 to 3 m thick and seems to have the same geometry than the topography; between 10 and 20 m, an area with a high possibility of saturated zone is identified. This zone, because of its probable high soil porosity, could act as a preferential water pathway, as it will be demonstrated in the next section.

4.2. Interpretation during the rain experiment

The methodology has then been applied on the geophysical profiles observed at different times during the rain infiltration experiment. For unconsolidated sediments such as the black marls soils, the V_s values vary generally slightly with an increase in water saturation [26,27]. The V_s tomograms were not included in the fusion process, and consequently the interpretation is only based on the H^*_1 hypothesis. The relative differences in the function H^*_1 have been computed for several time steps between times 1 (t_0) and 3 (12 h), 3 and 5 (24 h), 5 and 7 (36 h), 7 and 9 (48 h) and finally 9 and 11 (60 h). On Fig. 7, the water pathways during the rain infiltration are clearly identified. The variations of the possibility function on the right and left borders of the model are probably due to some artefacts associated with the electrical data inversion. Fig. 7a shows a superficial infiltration 12 h after the start of the experiment with a progressive saturation of the topsoil. In the next 12 h (time 5, Fig. 7b), the water continues to infiltrate more or less vertically into the top layer of the slope but the variations in soil saturation are still limited to the experimental plot where water is infiltrated at the surface. In the next 12 h (time 7, Fig. 7c), the value of possibility stops to increase at the vertical of the infiltration plot, but starts to increase at the downhill
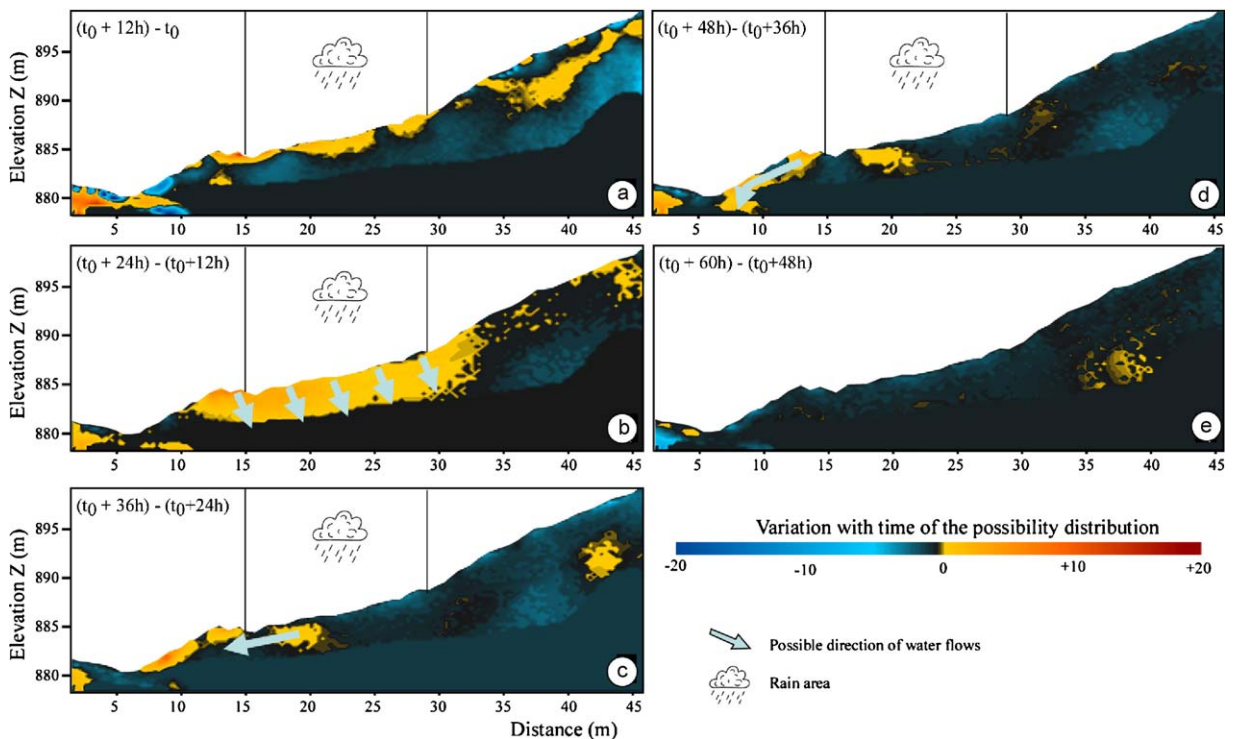

Fig. 7. Variations with time of the possibility distribution of meta-hypothesis H^*_2. a: variation between $t_0 + 12$ h and t_0 at the start of the infiltration experiment; b: variation between $t_0 + 24$ h and $t_0 + 12$ h; c: variation between $t_0 + 36$ h and $t_0 + 24$ h; d: variation between $t_0 + 48$ and $t_0 + 36$ h; e: variation between $t_0 + 60$ and $t_0 + 48$ h at the end of the infiltration experiment.

Fig. 7. Variations dans le temps de la fonction de possibilité H^*_2. a : entre les temps $t_0 + 6$ h et t_0 au début de l'expérience d'infiltration; b : Entre les temps $t_0 + 12$ h et $t_0 + 6$ h; c : Entre les temps $t_0 + 18$ h et $t_0 + 12$ h; d : Entre les temps $t_0 + 24$ et $t_0 + 18$ h; e : Entre les temps $t_0 + 30$ h et $t_0 + 24$ h à la fin de l'expérience d'infiltration.

edge of this plot. This may be interpreted as the onset of lateral water flow to the toe of the slope. In the next 12 h (time 9, Fig. 7d), the water continues to flow downhill in the subsurface but is guided by a drain to the base of the Laval stream. Finally, Fig. 7e shows no relevant changes with low variations in the possibility values. At time 11, the addition of water does not result in any variations in soil saturation, probably because the soil is fully saturated or because water infiltration is very limited and consequently the rain water is circulating by runoff at the surface. Fig. 7 also confirms two points:

- the base layer in the model (e.g. the blue-black contact in the figure) is certainly the impermeable marly bedrock since no variation is observed in this layer (this limit corresponds to the one identified in Fig. 6a when the possibility of the meta-hypothesis $H*_1$ is 0.65);
- the structure identified on Fig. 6b for a possibility value higher than 0.8 for the meta-hypothesis $H*_2$ is a drain (e.g. fissured area or less compacted area) as is clearly visible in Fig. 7d.

5. Conclusion

A combined geophysical approach based on seismic and electrical measurements has been conducted on a clay-shale slope in order to determine the internal structure, to identify some possible preferential water pathways and to monitor the water flow or changes in the soil saturation. The interpretation of V_p and V_s provides information on the state of compaction and on the porosity of the soil; the electrical resistivity (ρ) gives important indications on water contents. The changes of these parameters through time were measured during an infiltration experiment carried out on a portion of the slope. Geophysical tomograms were computed from the geophysical data and interpreted. To transfer the geophysical information to a thematic oriented one, a fusion technique is proposed in order to verify the possibility of different hypotheses related to hydrological processes within the slope. Meta-hypotheses, combining the possibility of the presence of fissures, high porosity areas and the possible development of saturated zones, were defined and computed. Analysis of these quantities reveals a more constrained model and highlights the presence of a drain which existence is confirmed by the hydrological observations. The relative differences between the possibility functions obtained at each time step are then calculated in order to monitor the water transfer within the slope. These results indicate that a fusion based on fuzzy set theory is an interesting tool for integrating geophysical interpretations for hydrological purposes. In particular, this method constitutes a real advance in multi-parameter methods compared to the qualitative methods classically used in geophysical interpretation, especially because the integration of likelihood functions in the fusion may guarantee that only reliable data are considered.

References

[1] P. Antoine, A. Giraud, M. Meunier, Th.W.J. van Asch, Geological and geotechnical of the « Terres Noires » in southeastern France: weathering, erosion, solid transport and instability, Engineering geology 40 (1995) 223–234.

[2] R.L. Baum, J. Messerich, R.W. Fleming, Surface deformation as a guide to kinematics and three-dimensional shape of slow-moving clay-rich landslides, Environmental engineering & geosciences 4 (1998) 283–306.

[3] A. Cras, V. Marc, Y. Travi, Hydrological behaviour of sub-Mediterranean alpine headwater streams in a badlands environment, Journal of Hydrology 339 (2007) 130–144.

[4] S.N. Domenico, Rock lithology and porosity determination from shear and compressional wave velocity, Geophysics 48 (1984) 1188–1195.

[5] D. Dubois, H. Prade, Fuzzy sets and systems: theory and applications, Academic Press, New York, 1980, 224p.

[6] J. Dvorkin, J.D. Walls, G. Mavko, Rock Physics of Marls, SEG Technical Program, Expanded abstracts (2001) 1784–1787.

[7] M. Fressard, O. Maquaire, J.P. Malet, S. Klotz, G. Grandjean, Morpho-structure and triggering conditions of the Laval landslide developed in clay-shales, Draix catchment (South French Alps). In: J.P. Malet, T.A. Bogaard, A. Remaître (Eds.), Landslide Processes, from geomorphologic mapping to dynamic modelling, CERG Editions, Strasbourg, 2009, pp. 107–110.

[8] T. Glade, P. Stark, R. Dikau, Determination of potential landslide shear plane depth using seismic refraction. A case study in Rheinhessen, Germany, Bulletin of geology and the environment 64 (2005) 151–158.

[9] G. Grandjean, Imaging subsurface objects by seismic p-wave tomography: numerical and experimental validations, Near surface geophysics 4 (2006) 275–283.

[10] G. Grandjean, A. Bitri, 2M-SASW: multifold multichannels seismic inversion of local dispersion of Rayleigh wave in laterally heterogeneous subsurfaces: application to the Super-Sauze mudslide (France), Near surface geophysics 30 (2007) 925–935.

[11] G. Grandjean, S. Sage, JaTS: a fully portable seismic tomography software based on Fresnel wavepaths and a probabilistic reconstruction approach, Computers and geosciences 30 (2004) 925–935.

[12] G. Grandjean, A. Bitri, C. Pennetier, O. Méric, J.P. Malet, Caractérisation de la structure interne et de l'état hydrique de glissements argilo-marneux par tomographie géophysique : l'exemple du glissement de terrain de Super-Sauze, C. R. Geoscience 338 (2006) 587–595.

[13] G. Grandjean, J.-P. Malet, A. Bitri, O. Méric, Geophysical data fusion by fuzzy logic for imaging the mechanical behaviour of mudslides, Bulletin de la société géologique de France 178 (2) (2007) 127–136.

[14] Y. Guéguen, V. Palciauskas, Introduction à la physique des roches, Hermann Ed, Paris, France, 1992, 299p.

[15] R.B. Herrmann, Computer programs in seismology, in : Department of Earth and Atmospheric Sciences, Saint-Louis University, USA, 2002.

[16] O. Hungr, S.G. Evans, M.J. Bovis, J.N. Hutchinson, A review of the classification of landslides of the flow type, Environmental engineering geoscience 7 (2001) 221–238.

[17] D. Jongmans, S. Garambois, Geophysical investigation of landslides: a review, Bulletin de la société géologique de France 178 (2) (2007) 101–112.

[18] M.H. Loke, The inversion of two dimensional resistivity data. PhD Thesis, University of Birmingham, Birmingham, UK, 1994, 122p.

[19] J.P. Malet, Les « glissements de type écoulement » dans les marnes noires des Alpes du sud. Morphologie, fonctionnement et modélisation hydromécanique, PhD Thesis, Université Louis-Pasteur, Strasbourg I, France, 2003, 394p.

[20] O. Maquaire, A. Ritzenthaler, B. Ambroise, Y. Thiery, E. Truchet, J.P. Malet, et al., Caractérisation des profils de formations superficielles par pénétrométrie dynamique à énergie variable : application aux marnes noires de Draix (Alpes-de-Haute-Provence, France), C. R. Geoscience 334 (2002) 835–841.

[21] R.D. Miller, J. Xia, C.B. Park, J. Ivanov, Multichannel analysis of surfaces waves to map bedrock, Leading edge 18 (1999) 1392–1396.

[22] A. O'Neill, M. Dentith, R. List, Full-waveform P-SV reflectivity inversion of surface waves for shallow engineering application, Exploration geophysics 34 (2003) 158–173.

[23] S.G. Park, S. Asano, S. Matsuura, T. Okamoto, J.H. Kim, Geoelectrical laboratory and field studies of groundwater occurrence in a landslide area: a case study from Japan, Exploration geophysics 36 (2005) 86–91.

[24] J.M. Reynolds, Application of geophysics to landslide investigations, in : Landslides and landslide management in North Wales, The National Museum and Galleries of Wales, Cardiff, 2002, pp. 28–30.

[25] D. Richard, N. Mathys, Historique, contexte technique et scientifique des BVRE de Draix. Caractéristiques, données disponibles et principaux résultats acquis au cours de dix ans de suivi, in : Actes du colloque « Les bassins versants expérimentaux de Draix, Laboratoire d'étude de l'érosion en montagne », Draix, Le Brusquet, Digne, France, 22-24 octobre 1997, Cemagref, Grenoble, France, 1999 .

[26] J.H. Schön, Physical properties of rocks. Fundamentals and principles of petrophysics, Handbook of geophysical explorations: Seismic exploration, 18, Pergamon Ed., Oxford, United Kingdom, 1996, p. 583.

[27] H. Stümpel, S. Kähler, R. Meissner, B. Milkereit, The use of seismic shear waves and compressional waves for lithological problems of shallow sediments, Geophysical prospecting 32 (4) (1984) 662–675.

[28] M.R.J. Wyllie, A.R. Gregory, L.W. Gardner, Elastic wave velocities in heterogeneous and porous media, Geophysics 21 (1956) 41–70.

[29] U. Yaramanci, Seismic surface waves in near surface geophysics, First break (2004) 4–6.

[30] L.A. Zadeh, Fuzzy sets, Information and control 8 (1965) 338–353.

[31] H.J. Zimmermann, Fuzzy sets and its applications, Kluwer Ed, Boston, USA, 1991, 544p.